A Satellite-Based Convective Cloud Object Tracking and Multipurpose Data Fusion Tool with Application to Developing Convection

JUSTIN M. SIEGLAFF, DANIEL C. HARTUNG, WAYNE F. FELTZ, AND LEE M. CRONCE

Cooperative Institute for Meteorological Satellite Studies, University of Wisconsin—Madison, Madison, Wisconsin

VALLIAPPA LAKSHMANAN

*Cooperative Institute for Mesoscale Meteorological Studies, University of Oklahoma, and
NOAA/National Severe Storms Laboratory, Norman, Oklahoma*

ABSTRACT

Studying deep convective clouds requires the use of available observation platforms with high temporal and spatial resolution, as well as other non–remote sensing meteorological data (i.e., numerical weather prediction model output, conventional observations, etc.). Such data are often at different temporal and spatial resolutions, and consequently, there exists the need to fuse these different meteorological datasets into a single framework. This paper introduces a methodology to identify and track convective cloud objects from convective cloud infancy [as few as three Geostationary Operational Environmental Satellite (GOES) infrared (IR) pixels] into the mature phase (hundreds of GOES IR pixels) using only geostationary imager IR window observations for the purpose of monitoring the initial growth of convective clouds.

The object tracking system described within builds upon the Warning Decision Support System-Integrated Information (WDSS-II) object tracking capabilities. The system uses an IR-window-based field as input to WDSS-II for cloud object identification and tracking and a Cooperative Institute for Meteorological Satellite Studies at the University of Wisconsin (UW-CIMSS)-developed postprocessing algorithm to combine WDSS-II cloud object output. The final output of the system is used to fuse multiple meteorological datasets into a single cloud object framework. The object tracking system performance analysis shows improved object tracking performance with both increased temporal resolution of the geostationary data and increased cloud object size. The system output is demonstrated as an effective means for fusing a variety of meteorological data including raw satellite observations, satellite algorithm output, radar observations, and derived output, numerical weather prediction model output, and lightning detection data for studying the initial growth of deep convective clouds and temporal trends of such data.

1. Introduction

Deep convective clouds develop on the order of minutes to hours. To observe the initial growth of deep convection, it is necessary to monitor these clouds with data at high temporal and spatial resolution. Geostationary imagers [e.g., Geostationary Operational Environmental Satellite (GOES), Spinning Enhanced Visible and Infrared Imager (SEVIRI), Japanese Advanced Meteorological Imager (JAMI)] are ideal instruments for investigating these clouds as they offer expansive spatial coverage (regional to full disk), high temporal resolution (5–15 min), and high spatial resolution (1–4 km) (Menzel and Purdom 1994; Aminou 2002; Puschell et al. 2002). Ground-based weather radar is another essential tool for examining the development of deep convection. In particular, the Next Generation Weather Radar (NEXRAD) network provides data at 5-min temporal resolution and very fine spatial resolution with coverage over the majority of the continental United States (CONUS) (NEXRAD 1985; Leone et al. 1989). In addition to remote sensing tools, forecasting and analyzing deep convection requires the integration of other meteorological datasets including, but not limited to, rawinsonde observations, surface observation networks,

numerical weather prediction (NWP) model guidance, lightning detection, and aircraft data (e.g., Benjamin et al. 1991; Johns and Doswell 1992; Moller 2001).

With the variety of available datasets at different spatial and temporal resolutions, there exists a need for an automated system that is capable of fusing the array of meteorological data types into a single framework. Working toward this goal, the University of Oklahoma developed the Warning Decision Support System-Integrated Information (WDSS-II; Lakshmanan et al. 2007b), which has been shown to successfully track radar-based objects through space and time using a variety of NEXRAD fields (Lakshmanan et al. 2003). Lakshmanan et al. (2007b) also showed that WDSS-II can be used for fusing a variety of meteorological data. For the purposes of this study, an "object" simply refers to a collection of adjacent data pixels grouped into a single entity and given a unique identification tag.

Creating and tracking convective objects using NEXRAD data requires a cloud to produce radar-detectable precipitation. However, clouds grow both vertically and horizontally prior to the detection of a corresponding radar echo. Therefore, it is beneficial to begin tracking satellite-derived cloud objects prior to significant NEXRAD-observed reflectivity since cloud growth rates can be used to nowcast storm development and future intensity ahead of such NEXRAD signatures (Roberts and Rutledge 2003).

Satellite-based object tracking systems have been developed to assist in the forecasting and nowcasting of convection and for fusing convective-related meteorological datasets. In particular, cloud object tracking systems such as the rapidly developing thunderstorms (RDTs; Morel et al. 2002), Maximum Spatial Correlation Tracking Technique (MASCOTTE; Carvalho and Jones 2001), and Forecast and Tracking the Evolution of Cloud Clusters (ForTraCC; Vila et al. 2008) algorithms are designed to identify convective cloud objects at the onset of maturity and continue tracking *throughout* the mature stage. These methods primarily focus on nowcasting the intensification and areal coverage of convection. Zinner et al. (2008) describes a daytime-only convective cloud object tracking system [Cumulonimbus Tracking and Monitoring (Cb-TRAM)] designed to diagnose convective cloud initiation and growth by fusing satellite observations and NWP model information. However, Cb-TRAM is not capable of retaining a history of the properties of multiple meteorological fields through a cloud object's lifetime. Unlike the above satellite-based tracking methods, WDSS-II offers the capability to track and retain historical properties for individual cloud objects at any user-defined stage of the convective life cycle.

Lakshmanan et al. (2009) demonstrated that it is possible to identify objects within WDSS-II using satellite imager infrared (IR) window brightness temperatures. This study presents a convective cloud object identification and tracking system that utilizes a single geostationary satellite IR-window-based field, the 11-μm top-of-troposphere cloud emissivity (ε_{tot}; Pavolonis 2010b). This convective cloud object tracking system employs the WDSS-II framework and an additional postprocessing utility developed at the Cooperative Institute for Meteorological Satellite Studies at the University of Wisconsin (UW-CIMSS). The goal in developing this system is to mimic a human's subjective interpretation of cloud objects in an objective automated manner.

The satellite-based convective cloud object identification and tracking system presented herein is unique in many ways. First, the system is designed to monitor the *growth* stage of convective clouds from infancy (as few as three GOES IR pixels) to satellite maturity (hundreds of GOES IR pixels). While it is important to monitor these clouds from infancy through decay, this system is particularly designed to monitor the early growth of these clouds (from infancy into the mature phase). Second, the tracking system input (ε_{tot}) is derived from IR satellite observations, allowing for operation both day and night. Moreover, ε_{tot} does not rely on brightness temperature (BT) thresholds; this permits the full range of the input data to be processed and for the *object identification to remain independent of season and latitude*. Finally, the convective cloud object tracking system is multipurpose, in that it can be used to validate convective initiation algorithms with respect to other meteorological data fields from an object-based perspective, to conduct basic research for further understanding the growth stage of deep convection, and to serve as a foundation for a convective initiation (CI) nowcasting tool. This paper is organized in the following format: 1) data used, 2) a comprehensive description of convective cloud object tracking system components, 3) an analysis and discussion of system performance, 4) an example using the system, and 5) concluding remarks.

2. Data

High temporal resolution geostationary imager data are input into the convective cloud object tracking system. In this paper, *GOES-12* imager data over the central and eastern CONUS and adjacent oceanic regions (bounded by approximately 25°–52°N, 108°–65°W) are used to demonstrate and test the performance of the system for 34 convectively active periods during 2008 and 2009 [periods selected include both daytime and
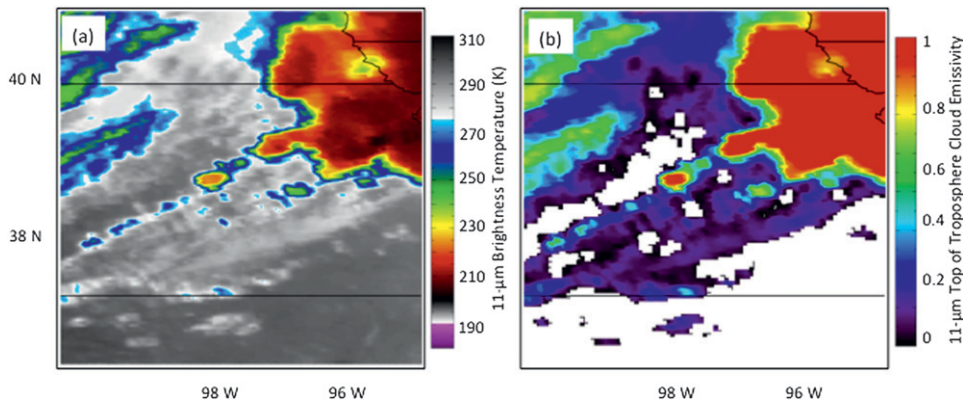
FIG. 1. (a) *GOES-12* 11-μm BT and (b) corresponding 11-μm top-of-troposphere cloud emissivity valid at 2002 UTC 15 May 2009.

nighttime scenes; specific dates/times can be found in Sieglaff et al. (2011)]. The temporal resolution of the *GOES-12* imager data varies from 5 to 30 min depending on the GOES scanning strategy, with 10–17-min temporal resolution as the most common.

The input dataset for the WDSS-II component of the convective cloud object tracking system is the 11-μm top-of-troposphere cloud emissivity (ε_{tot}; Pavolonis 2010b) and is given by the following equation:

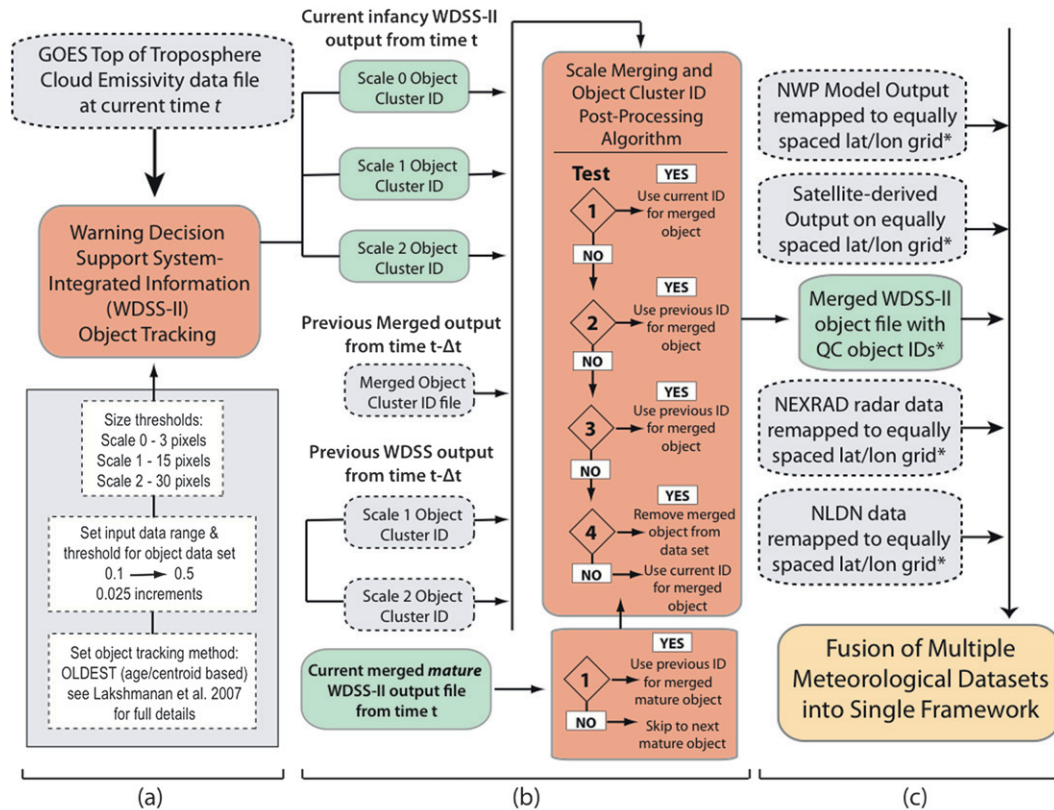$$\varepsilon(\lambda) = \frac{R_{obs}(\lambda) - R_{clr}(\lambda)}{[B(\lambda, T_{eff})T_{ac}(\lambda) + R_{ac}(\lambda)] - R_{clr}(\lambda)},$$

where $R_{obs}(\lambda)$ is the observed 11-μm radiance, $R_{clr}(\lambda)$ is the clear-sky 11-μm radiance from a radiative transfer model, and the term in the square brackets represents the blackbody cloud radiance that is transmitted to the top of atmosphere plus the above-cloud atmospheric radiance. The $T_{ac}(\lambda)$ and $R_{ac}(\lambda)$ above-cloud terms are supplied from a radiative transfer model. All radiative transfer model calculations in the above equation are computed with temperature and moisture profiles inputs from the Global Forecast System (GFS; Kanamitsu 1989). Full details of the computation of ε_{tot} can be found in Pavolonis (2010b) and are out of the scope of this manuscript.

Practically, the ε_{tot} can be described as a background-corrected emissivity (clear-sky absorption and surface emissivity) that a cloud would exhibit if it were located at the tropopause and is thus calculated for all satellite pixels determined to be cloudy by a cloud mask (Heidinger, 2010). The unitless values range from 0.0 to 1.0, where 1.0 signifies that the cloud is at or above the tropopause and a value near 0.0 is indicative of a cloud just above the earth's surface. A value of 0.5 represents a cloud half way between the ground and tropopause. The ε_{tot} employs the tropopause height extracted from

the GFS output, although any NWP model data could be used. Spatially, the ε_{tot} maintains the gradients observed in the 11-μm BT field; but unlike BT, the ε_{tot} field is nearly independent of season and latitude. Therefore, ε_{tot} was chosen over the IR BT for cloud object creation. For example, a mature convective cloud near the tropopause will always have ε_{tot} values approaching 1.0,[1] whereas the BT of such a cloud can vary on the order of tens of kelvins both latitudinally and by season.

Figure 1 shows an example of the ε_{tot} field compared to the IR window BT field. It is evident that spatial gradients observed in the BT field are preserved in the ε_{tot} field for nonmature thunderstorm anvils. Mature thunderstorm anvils have ε_{tot} values approaching 1.0, signifying that they are at or near the tropopause (Fig. 1). The apparent lack of spatial gradients within the ε_{tot} field within mature thunderstorm anvils is not problematic (the lack is partially the color enhancement chosen and partially an actual reduction of spatial gradients for areas at or above the model tropopause). As will be elaborated on later in the text, the developed configuration of WDSS-II for cloud object creation requires the grouping of middle/upper-tropospheric ε_{tot} values into a single group, thus a lack of horizontal contrast does not detrimentally impact object creation. Within this system, contrast in the higher range of ε_{tot} values is not important because 1) we do not seek to isolate cold areas atop existing convection, but rather to monitor the earlier growth of convective clouds; and 2) the manipulation of the ε_{tot} field is purely for object creation; the full unaltered ε_{tot} field is simultaneously retained within cloud objects for use in data analysis.

---

[1] The 11-μm top-of-troposphere cloud emissivity has an upper bound of 1.0 and thus is limited to 1.0 in cases where the NWP model incorrectly underforecasts the tropopause height.

FIG. 2. High-level flowchart illustrating the procedure of the convective cloud object tracking system. (a) WDSS-II configuration and object building and tracking component of the system. (b) Postprocessing system. (c) Fusion of multiple meteorological datasets into a single cloud object framework.

3. Convective cloud object tracking methodology

The convective cloud object tracking system is broken down into two main components: 1) a WDSS-II component that uses ε_{tot} for cloud object generation and initial tracking and 2) a UW-CIMSS-developed postprocessing system that reduces broken convective cloud object tracks. A high-level flowchart of the processing system is shown in Fig. 2 and is referenced throughout section 3. The output from the convective cloud object tracking system and statistical postprocessing methodology can be used to fuse any type of meteorological data with the cloud object framework.

a. WDSS-II using ε_{tot}

WDSS-II is a data manipulation system with many utilities; all references to WDSS-II throughout the remainder of the text are simply referring to its object creation and tracking capabilities. WDSS-II can build cloud objects at any number of user-specified size scales using the enhanced watershed transform method

(Lakshmanan et al. 2009) and also provides a variety of options for tracking cloud objects through space and time. The WDSS-II cloud object creation and tracking process is discussed in moderate detail throughout the remainder of this section; for complete details on the WDSS-II object identification algorithm, the reader is referred to Lakshmanan et al. (2003, 2009).

In our configuration, the ε_{tot} field is processed by WDSS-II on three spatial scales (Fig. 2a). Each scale refers to the *minimum number of pixels* that a cloud object must achieve before the growth is terminated by WDSS-II on that particular scale. The description of the three scales is fully described later in this section, but it is worth noting that the three scales are required to 1) capture very small objects, 2) improve tracking by having larger scale objects, and 3) ensure that cloud objects encompass as much of a developing cloud as possible. In addition, if a cloud object does not achieve the minimum number of pixels required for a given scale, it is pruned by the enhanced watershed technique (Lakshmanan et al. 2009). WDSS-II builds cloud objects on each scale by first determining all local maxima in the ε_{tot} input

field. Each cloud object is then filled from the local maxima to smaller values of ε_{tot} based upon the user-configured data depth and scale size thresholds. It should be noted that the configuration discussed here was chosen heuristically after testing multiple configurations; the results of each individual test configuration are not shown. Although the system is referred to as a convective cloud object tracking system, all clouds (ε_{tot} values) are input into WDSS-II for object creation and tracking. The WDSS-II configuration described below is specifically tailored for tracking convective clouds from infancy to maturity; we are not concerned with the object tracking performance for synoptic-scale cloud systems, clouds associated with jet streaks, or large cirrus shields.

Cloud objects are grown within WDSS-II from the local maxima in the ε_{tot} field by first grouping continuous pixels with ε_{tot} values greater than 0.5 into unique clusters. This step of grouping values between 0.5 and 1.0 is done to maximize computational efficiency and to define middle- to upper-tropospheric cloud features as single entities. This configuration does not seek to capture small areas within a developing thunderstorm anvil, but rather is designed to encompass the entire developing thunderstorm tower and anvil in one cloud object. The cloud object building continues on each scale in 0.025 increments for ε_{tot} values between 0.50 and 0.10. Each cloud object on a given scale grows until the minimum size threshold for that scale is achieved. Cloud objects that cannot be grown further and do not achieve the minimum size for particular scales are pruned. The small bin size (0.025) for lower- to middle-tropospheric clouds is chosen to keep cloud objects from spatially growing too large (i.e., merging features into large objects that a human analyst would consider separate entities).

Cloud objects are grown on three scales: 3, 15, and 30 pixels [the pixels are a 0.04° grid, which is approximately the resolution of the input GOES imager 4-km IR data (Menzel and Purdom 1994)]. After testing a range of sizes (analysis not shown), the above combination yielded the best performance. The smallest scale (three pixels, ~4–8 km on a side) is necessary to capture convective clouds in the very early stages of growth. The two larger scales (15 and 30 pixels, ~28 and 60 km on a side) allow cloud objects to grow large enough to encompass the vast majority of the developing convective cloud. These multiple scales are designed to resolve convective clouds at different stages of growth from infancy to maturity. A single WDSS-II output scale by itself is not sufficient for capturing all phases of convective cloud growth, and it is therefore necessary to combine all three WDSS-II output scales into a single, merged set of cloud objects through a postprocessing step.

Within WDSS-II, cloud objects are assigned unique object identification (ID) numbers and tracked across space and time. WDSS-II offers several options for tracking cloud objects. Many of the WDSS-II object tracking options do not rely on object overlap between two times, but rather minimize a cost function [Thunderstorm Identification, Tracking, Analysis, and Nowcasting (TITAN); Dixon and Wiener 1993; Lakshmanan and Smith 2010] for a given object at one time versus candidate objects at the following scan time. The reader is referred to Lakshmanan and Smith (2010) for a complete description of WDSS-II object tracking methods.

The WDSS-II *oldest* (Lakshmanan and Smith 2010) object tracking option was determined most skillful for our application, with preference for maintaining the oldest cloud object when multiple candidates exist within a user-defined tolerance distance. Since the primary utility of this system is to investigate relationships between real-time, historical, and forecast datasets for individual evolving cloud objects, methods such as Multiple Hypothesis Tracking (MHT; Root et al. 2011), which allow for the modification of historical object tracks based on current information, are not applicable to this work. The WDSS-II oldest object tracking methodology uses a user-configurable search radius for each scale. The search radius configuration selected for the convective cloud object tracking system is equal to the greater of the object radius and 20 km. The radius of a cloud object is defined as the radius of a circle with the same total area of the cloud object. WDSS-II uses an object's centroid location and search radius to look for companion objects; in other words, an object's centroid from one time to the next must be within the search radius to be successfully tracked (unique object ID number maintained between two times). The dynamic *and* 20-km maximum search radii thresholds allow small objects to be successfully maintained between GOES imager scans. Additionally, the WDSS-II user configuration specifies to only consider adjacent times when tracking objects [e.g., an object ID number is not allowed to coast (disappear and then later reappear at a later time)].

The two-dimensional fields for each of the three cloud object scales (and their associated object ID numbers) are then combined in a postprocessing step to create one unique set of merged objects. An example of the three individual WDSS-II cloud object scales and the final postprocessed merged objects valid at the same time as Fig. 1 (2002 UTC 15 May 2009) are shown in Fig. 3. Figure 3a illustrates the ability of small convective objects to be identified on scale 1. Some of the small objects on scale 1 are part of larger objects on scales 2 and 3 (Figs. 3b,c) (e.g., cloud along the Kansas–Oklahoma
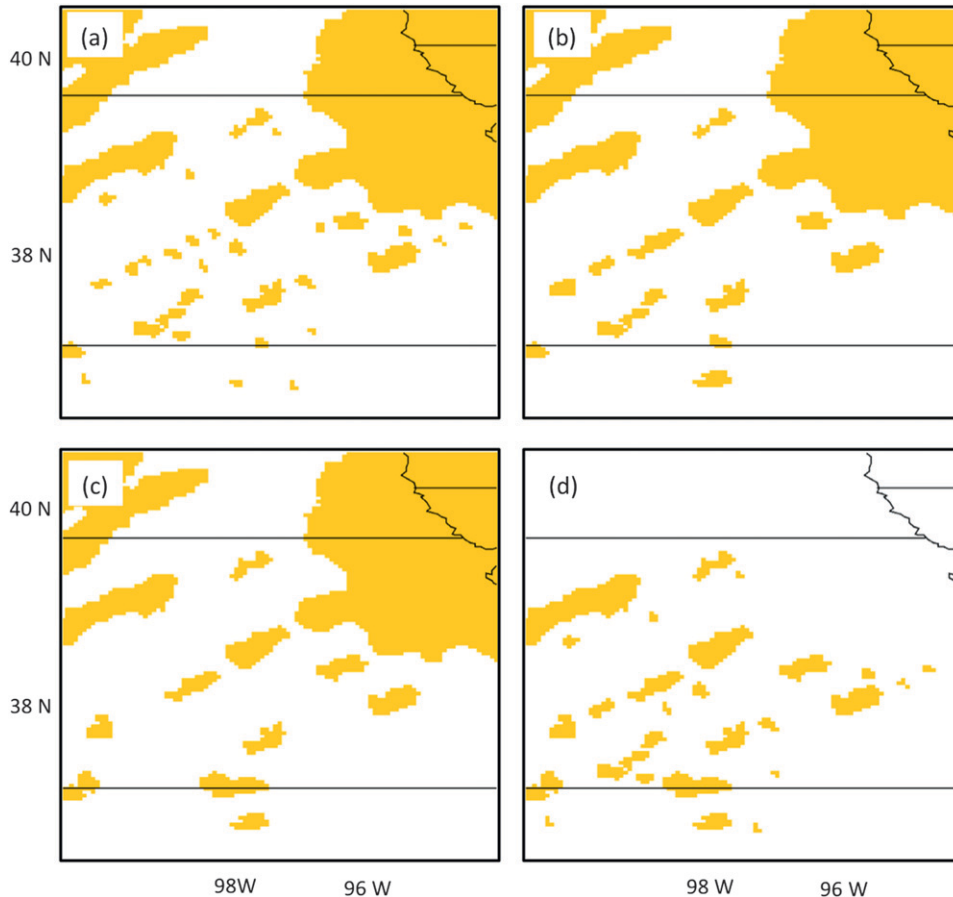
FIG. 3. WDSS-II (a) scale 1, (b) scale 2, and (c) scale 3 objects and ID numbers valid at 2002 UTC 15 May 2009. (d) The final merged cloud objects' output from the UW-CIMSS postprocessing system valid at the same time. These cloud objects correspond to the satellite imagery in Fig. 1.

border at ~98°W), while other objects are unique to scale 1. The UW-CIMSS postprocessing component of the system that combines the three WDSS-II scales (Fig. 3d) is fully described in the following section.

b. Cloud object postprocessing system

1) MAIN CLOUD OBJECT POSTPROCESSING

After WDSS-II cloud object creation and tracking are complete, a postprocessing routine combines the three cloud object scales into a set of final merged objects at each time. These merged cloud objects are used for fusing meteorological data (Fig. 2b) into a single framework. This postprocessing step is an essential part of the system as it ensures that cloud objects encompass the fullest possible extent of a convective cloud while not allowing objects to grow spatially unbounded, similar to how a human would identify convective cloud objects. In addition to merging the three WDSS-II scales into a set of final cloud objects, a series of tests are

conducted to assign and maintain temporally consistent object ID numbers between consecutive satellite scans. This step is critical when the WDSS-II object tracking fails and a cloud object undesirably changes ID between two satellite scans. The main cloud object postprocessing procedure is described in detail below and in Table 1. Also, two user options of the postprocessing methodology are briefly described. Upon completion of the cloud object postprocessing, object properties and any associated meteorological data for each object are retained for each time step that the cloud object exists.

The postprocessing algorithm loops through the cloud objects on scale 1 (smallest scale) in descending order of maximum cloud object ε_{tot}. Each cloud object on scale 1 is potentially grown larger by combining overlapping objects on the larger scales 2 and 3. The newly grown cloud object is stored as a temporary merged cloud object (Table 1: steps 1–3d) and is assigned the scale 1 object ID number so long as the particular ID number is not already in use. It is necessary to use the object ID number from

TABLE 1. Detailed description of the main component of the UW-CIMSS postprocessing system.

Main Cloud Object Postprocessing Procedure
1) For t_{curr}, generate 2D temporary merged cloud object array and initialize to -9999 (missing values)
2) If $t_{curr} \neq$ the first processing time, then load WDSS-II scale 2, scale 3, and final merged objects for t_{prev}
3) Generate an index of scale 1 cloud object ID numbers at t_{curr} sorted in descending order of maximum 11-μm top-of-troposphere cloud emissivity (ε_{tot}), count_sort
- If count_sort > 0, then loop over index generated in (3)
a) Use scale 1 cloud object footprint as the initial temporary merged cloud-object at t_{curr}
- If scale 1 object ID number is not already in use at t_{curr}, then
$\rightarrow$ assign scale 1 object ID number to temporary merged cloud object
- Else $\rightarrow$ assign ID number of -333 to temporary merged cloud object
b) Use object footprint to determine which scale 2 cloud objects overlap with temporary merged cloud object at t_{curr}, num_overlap2
- If num_overlap2 > 0, then
$\rightarrow$ grow temporary merged cloud object to include overlapping scale 2 cloud objects
c) Use object footprint to determine which scale 3 cloud objects overlap with temporary merged cloud object at t_{curr}, num_overlap3
- If num_overlap3 > 0, then
$\rightarrow$ grow temporary merged cloud object to include overlapping scale 3 cloud objects
d) If temporary merged cloud object > maximum allowed object size (1000 pixels), then purge temporary cloud object; ELSE continue
- If $t_{curr} \neq$ first processing time, then begin
e) Create index of final merged object ID numbers at t_{prev} that overlaps with object footprint at t_{curr}, ct_pre
- If ct_pre > 0, then for each overlapping final merged cloud object at t_{prev}:
i) Retrieve WDSS-II scale 2 and scale 3 object ID numbers at both t_{prev} and t_{curr}
ii) Test to see if the WDSS-II scale 2 or scale 3 ID number is consistent between t_{prev} and t_{curr}
- END Subroutine
- If at least one final merged cloud object at t_{prev} has a temporally consistent WDSS-II scale 2 or scale 3 ID number, then begin
i) Find the temporally consistent object ID number that has the maximum areal overlap with the t_{curr} temporary final merged object and is not already in use
ii) If all overlapping final merged object ID numbers at t_{prev} are in use, then the temporary merged cloud object at t_{curr} is purged
- END Subroutine
- END Subroutine
f) If a temporary merged object ID number of -333 was not replaced through the previous series of tests, then purge object
- END Routine

the smallest scale since small objects (less than 15 pixels) will only be identified on scale 1. After these steps, should an object exceed 1000 pixels ($\sim$17 600 km^2), the object is purged. This purging increases efficiency and also eliminates large, mature convective systems that are not targeted by this cloud object tracking system.[2]

---

[2] Convective clouds growing beneath cirrus clouds are identified and tracked if the cirrus clouds are sufficiently thin. Given the WDSS-II configuration used, this equates to convective clouds developing beneath cirrus clouds with ε_{tot} values less than 0.50; practically, these are generally cirrus clouds in which you can see lower clouds in visible channel observations. For convective clouds developing beneath thicker cirrus clouds, such as thick thunderstorm anvils, the cirrus clouds effectively obscure any growing convection and therefore a unique object is not created for these new convective towers. Often these large areas of thick cirrus clouds exceed the system's upper size limit and are purged.

A consequence of how the merged object field is populated (i.e., descending order of maximum ε_{tot}), it is possible for a scale 1 ID number to have been assigned at a previous time. Since it is imperative that two objects never be assigned the same final merged object ID number, if the scale 1 object ID number is already in use within the field of temporary merged cloud objects, then the temporary merged object is assigned a temporary placeholder ID number. The procedure for reassigning object ID numbers with a temporary placeholder ID number is discussed later.

One limitation of the WDSS-II object tracking system is that it has the highest failure rate for scale 1 objects because of their small spatial extent, rapid storm evolution during the growth stage, and a potentially large distance traveled during GOES scan gaps relative to their size (i.e., especially 3-hourly, 30-min temporal data gaps due to GOES full-disk scans). In this context,

failure refers to when a scale 1 object incorrectly changes ID between the previous (t_{prev}) and current (t_{curr}) satellite scan times. Further analysis of this assertion is explored in section 3c. To overcome these challenges, a series of tests were devised within the UW-CIMSS postprocessing algorithm that utilizes the final merged cloud object field at t_{prev} and the WDSS-II cloud objects on scales 2 and 3 at t_{prev} and t_{curr} to assign final merged object ID numbers at t_{curr}.

As step 3e (Table 1) initially identifies all final merged cloud objects at t_{prev} that spatially overlap with the temporary merged cloud object, similar to the overlap association technique used by Morel et al. 1997, it is assumed that any object at t_{prev} that overlaps with the temporary merged cloud object at t_{curr} *may* be the same object; these objects are termed "candidate objects." The WDSS-II object tracking (and associated object ID assignment) in our application improves for scales 2 and 3 relative to scale 1 (further discussed in section 3c). This improvement stems from cloud objects on scales 2 and 3 being larger and, consequently, less sensitive to the distance traveled between GOES scans relative to the object tracking search radius. Each candidate object is tested for WDSS-II scale 2 or scale 3 "consistency" between t_{prev} and t_{curr}. Any object that has the same scale 2 or scale 3 object ID number at t_{prev} and t_{curr} exhibits consistency and is retained, while all others are no longer considered. The areal overlap between the temporary merged object and the remaining candidate objects is computed. Finally, the temporary merged cloud object is assigned the ID number of the candidate object that has the most areal overlap and whose ID number is not already in use within the temporary merged cloud object field. If no candidate objects qualify, then the object is purged.

If the WDSS-II scales and final merged cloud object fields do not exist at t_{prev}, (e.g., the first time step when running the convective cloud object system), then step 3e in Table 1 is skipped and processing continues with step 3f. Table 1, step 3f simply purges objects that were initially assigned a placeholder ID number and were not reassigned an object ID number by the aforementioned tests (e.g., their temporary merged object did not overlap with any unused final merged cloud objects at t_{prev}).

2) USER OPTION: MATURE OBJECT EXTENSION

Since a key motivation for developing this convective cloud object tracking system was to fuse a variety of meteorological datasets to study the growth and maturation of deep convection, it is desirable to track final merged objects into the mature phase of the thunderstorm life cycle. One research project at UW-CIMSS utilizes this system to validate the University of Wisconsin Convective Initiation–Cloud-Top Cooling (UWCI-CTC) algorithm (Sieglaff et al. 2011) against a variety of NEXRAD fields. Initial results of this project have suggested that even though a number of final merged cloud objects achieved a moderate to strong radar reflectivity (40–50 dBZ), many failed to strengthen to intense reflectivity values (55+ dBZ). It is understood that each convective cloud object that develops a 45-dBZ radar echo will not necessarily intensify to 60 dBZ; however, the drop off in sample size between the two reflectivity classifications was larger than expected given the convectively active periods that were being evaluated. Further investigation revealed that many convective cloud objects were merged into conjoined larger objects due to spatially connected thunderstorm anvils. These much larger cloud objects were then purged since their size exceeded the maximum 1000-pixel size threshold described in section 3b(1).

The top–down satellite observations, in combination with horizontal anvil expansion, prevented the objects from being treated as individual entities for a sufficient amount of time. To address this problem from a validation perspective, an option was added to the UW-CIMSS postprocessing methodology that tracks the core of mature thunderstorms for one to four additional GOES imager scans than was otherwise possible with the system. This was added as an option to the system, especially for situations where transitioning a cloud object from encompassing an entire convective cloud to only the core of the convective cloud is not detrimental. For example, in a validation type study when collocating satellite algorithm and radar signals within a cloud object is necessary to compute probability of detection (POD) and probability of false detection (POFD) statistics, this option is desirable; however, it is undesirable for other tasks, such as objectively quantifying the areal size or rate of areal expansion of a cloud object with time.

The implementation of the mature object extension uses a secondary WDSS-II cloud object tracking configuration and similar overlap concepts as discussed in section 3b(1) (Fig. 2b), except that it only focuses on ε_{tot} values greater than or equal to 0.90 and uses slightly larger size thresholds for the three cloud object scales (20, 40, and 60 pixels). Objects from the mature object extension are added to the final merged cloud object field produced in section 3b(1). The new object is assigned the final merged object ID number from t_{prev} that exhibited maximum overlap with the mature extension object and does not already exist in the final merged cloud object field at t_{curr}. Should no object meet

the above-mentioned criteria, the mature extension object is not included in the final merged cloud object field.

3) USER OPTION: MERGED OBJECT ABSORPTION

When using the cloud object tracking system as a validation tool, it is essential to identify when two cloud objects at t_{prev} merge into one cloud object at t_{curr}. The following scenario further illustrates this point: Two adjacent developing thunderstorms are each characterized by a unique final merged object ID number at t_{prev}, a satellite indication of convective cloud growth (i.e., a cooling cloud-top signal), and have an observed radar reflectivity of 35 dBZ. At t_{curr}, the two cloud objects merge into a single cloud object (maintaining one of the two object ID numbers). The maintained cloud object at t_{curr} continues to be tracked in space and time and eventually develops a 60-dBZ reflectivity on radar. In a validation framework, the object ID number that was tracked until it developed a 60-dBZ reflectivity echo would count as a "hit" for that particular reflectivity threshold. However, the object that disappeared as a result of merging would count as a miss for all reflectivity thresholds in excess of 35 dBZ when in actuality, it may have strengthened on radar after the two satellite objects at t_{prev} merged. Therefore, it is important to define an attribute for each final merged cloud object that identifies if and when it merges with another object in order for validation statistics to dismiss such objects upon absorption. To address this need, the UW-CIMSS postprocessing system has incorporated a merged object absorption option that identifies the time that an object is absorbed by another object at t_{curr}.

After the t_{curr} final merged object field has been created as described by section 3b(1) [and optionally section 3b(2)] and when final merged objects at t_{prev} are available (e.g., not the first time in a processing sequence), each final merged object at t_{prev} is checked for existence within the t_{curr} final merged object field. The object ID numbers at t_{prev} that do not exist at t_{curr} are inspected further. If an object at t_{prev} overlaps with an object at t_{curr}, yet that object ID number does not exist at t_{curr}, then it is assigned an absorbed time of t_{curr}. The object absorption also accounts for objects that existed at t_{prev} but do not exist at t_{curr} and do not reside within an object at t_{curr} because of the object exceeded the maximum size threshold. In these cases, the ε_{tot} field is sampled at the t_{prev} footprint; if the maximum ε_{tot} at t_{curr} within the t_{prev} footprint is greater than or equal to 0.50, then the object is considered to have been absorbed into an object at t_{curr} that exceeded the maximum object size threshold and
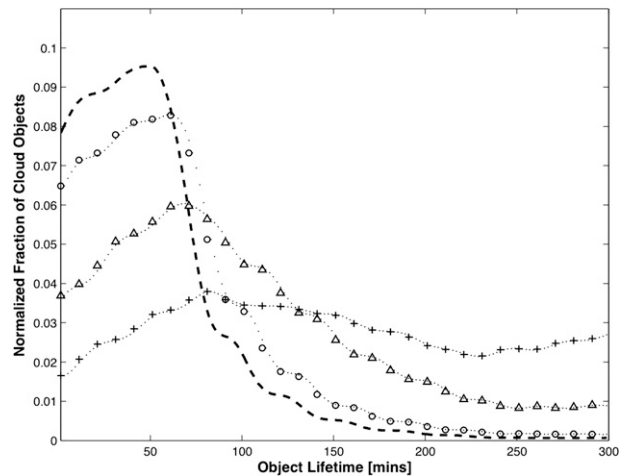

FIG. 4. Distribution of cloud object lifetime (min) as a function of the maximum 11-μm top-of-troposphere cloud emissivity (ε_{tot}) achieved during object lifetime. The following ε_{tot} bins are shown: $0.2 < \varepsilon_{tot} \leq 0.3$ (dashed line, - -), $0.4 < \varepsilon_{tot} \leq 0.5$ (dashed circles, -o-), $0.6 < \varepsilon_{tot} \leq 0.7$ (dashed triangles, -Δ-), and $\varepsilon_{tot} \geq 0.9$ (dashed pluses, -+-). These data are populated from 34 convectively active periods over the central and eastern United States during the spring and summer of 2008 and 2009.

hence was purged.[3] These cloud objects at t_{prev} are assigned an absorbed time of t_{curr}.

c. Discussion of convective cloud object tracking performance

One metric for determining the performance of the cloud object tracking system is the amount of time (in minutes) that cloud objects are successfully tracked as a function of the maximum ε_{tot} achieved during the object's lifetime (Fig. 4). Figure 4 and Table 2 show that as cloud objects grow higher into the troposphere (and, consequently, exhibit larger ε_{tot} values), the mean lifetime increases from ~35 min for cloud objects remaining in the lower troposphere (maximum ε_{tot} between 0.20 and 0.30) to near 155 min for cloud objects approaching the tropopause (maximum ε_{tot} greater than 0.90). The progression to longer lifetimes for objects with increased vertical development is consistent with the concept that a cumulonimbus is more organized and hence longer lived than a towering cumulus, and likewise a towering cumulus is more organized and often longer lived than a shallow cumulus cloud (Wallace and Hobbs 1977). The distributions of object

---

[3] An ε_{tot} value of 0.50 was chosen because the primary WDSS-II object configuration groups all values of ε_{tot} between 0.50 and 1.0 into the first WDSS-II processing bin. Therefore, any values within this range must reside in the same object unless the object exceeded the maximum allowed size and was hence purged.

TABLE 2. Mean and standard deviation of the lifetime (min) of cloud objects from the distributions shown in Fig. 4. Cloud objects are binned according to the maximum 11-μm top-of-troposphere cloud emissivity value achieved during their lifetime. These data are populated from 34 convectively active periods over the central and eastern United States during the spring and summer of 2008 and 2009.

Max object ToT emissivity (ε_{tot})	Mean lifetime (min)	Std dev (min)
$0.2 < \varepsilon_{tot} \leq 0.3$	35.2	37.8
$0.4 < \varepsilon_{tot} \leq 0.5$	46.8	47.3
$0.6 < \varepsilon_{tot} \leq 0.7$	91.0	78.1
$\varepsilon_{tot} \geq 0.9$	155.9	108.3

lifetime are much wider for convective cloud objects near the tropopause (thunderstorms) than lower tropospheric cloud objects (shallow cumulus fields) (Fig. 4). In fact, the cloud object lifetime distribution for thunderstorms (cloud objects with maximum ε_{tot} greater than 0.90) weakly peaks near 80 min with a substantial tail extending to 300+ min. An analysis of thunderstorm cloud objects (not shown) suggests that the weak peak near 80 min can be attributed to storms that develop in linear regimes and merge into large anvil objects that eventually become pruned; the linear convection from 15 May 2009 in Fig. 3 is one such example. Thunderstorm cloud objects lasting for more than 120 min consist largely of isolated storms, often dryline scenarios or initial cells in linear regimes. These distributions lend confidence that the convective cloud object tracking system is performing as expected.

A strength of the cloud object tracking system is that it can be used with data from any geostationary satellite platform (with sufficient temporal resolution). The ε_{tot} field is computed using 11-μm IR observations measured by all operational geostationary imagers (GOES, Menzel and Purdom 1994; SEVIRI, Aminou 2002; JAMI, Puschell et al. 2002, etc.) and the Heidinger (2010) cloud mask is adaptive to the different available spectral channels on various satellite imagers.

In general, as the temporal resolution of the satellite increases, the cloud object tracking becomes more accurate. Current GOES imagers have a routine temporal resolution of ~15 min over CONUS (alternating between 13- and 17-min scans); though in cases of expected severe convection or other high-impact weather, rapid scan mode is invoked, providing up to 5-min temporal resolution over CONUS (Hillger and Schmit 2007). Independent of the GOES scan mode, 30-min gaps occur every 3 h (beginning at 0000 UTC) because of scheduled full-disk scans. The 30-min gaps can be a significant source of error in the cloud object tracking system, especially for spatially small objects and objects that grow tremendously within those 30-min periods. Convective cloud objects that have already developed an anvil are typically tracked successfully through these 30-min temporal gaps.

Figure 5a demonstrates how the temporal resolution of a GOES scan pattern impacts the convective cloud object tracking system performance. For periods in which GOES is in rapid scan mode (temporal gap of 10 min or less), the object tracking performs best with 69% of cloud objects retained following a rapid scan gap (Fig. 5a). As the temporal resolution of the satellite coarsens, the object tracking performance degrades with the cloud object retention rate decreasing to 59% for the GOES routine scan mode (13–17-min scan gaps) and 40% for more than 20-min GOES scan gaps (Fig. 5a). The absolute retention rates are not necessarily important since the baseline rate is not quantified; however,
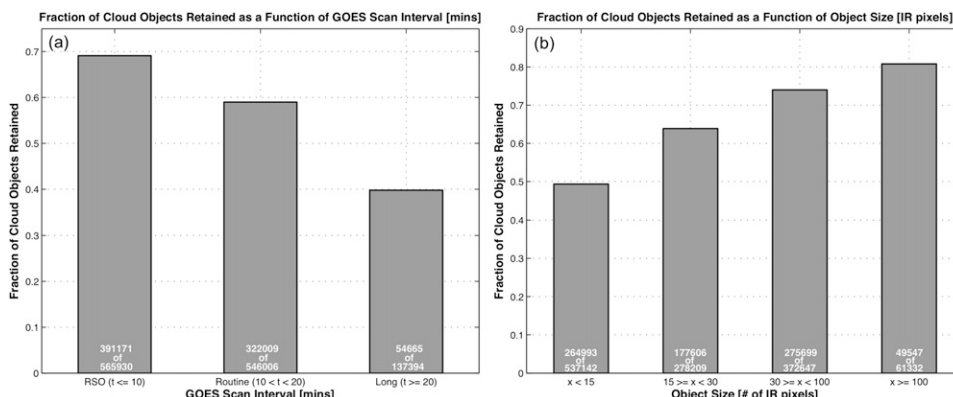

FIG. 5. Cloud object retention rate as a function of (a) GOES scan interval and (b) cloud object size. Cloud object sample size of each group is indicated at the bottom of each bar. Cloud objects are taken from 34 convectively active periods during 2008 and 2009 over the central and eastern United States and adjacent oceanic regions.

the overall increase in retention rate with increased satellite temporal resolution is noteworthy.[4] The future GOES Advanced Baseline Imager (ABI) on board GOES-R will provide 5-min temporal coverage over CONUS and at least 15-min coverage over the full disk (possibly 5-min full disk, depending on which scanning pattern is chosen) (Schmit et al. 2005). Based on the above-mentioned analysis, the increased temporal sampling of GOES-R ABI will greatly reduce the errors associated with the cloud object tracking system. Though not extensively tested nor shown in the text, this cloud object tracking system has been initially tested with SEVIRI data (15-min full-disk coverage) with encouraging results. Porting to other operational geostationary imagers is also possible, although this has not been exercised. However, it is recommended that the imager have predominately 15-min or better temporal resolution to successfully use the tracking system.

As referenced in section 3b(1), the spatial size of cloud objects also impacts the system performance. Previously, it was stated that a limitation of the WDSS-II object tracking system is that it has the highest failure rate for scale 1 objects because of their small spatial extent, rapid storm evolution in the growing stage of convection, and potentially large distance traveled during GOES scan gaps. Figure 5b shows the convective cloud object retention rate as a function of cloud object size in number of pixels. The smallest objects (less than 15 GOES IR pixels) that only exist on scale 1 exhibit the lowest retention rate (49%), and the retention rate increases as the cloud object size increases (Fig. 5b). For cloud objects with at least 15 pixels but less than 30 pixels (objects that exist on scales 1 and 2), the retention rate increases to 64%. A similar upward trend is observed for cloud objects with at least 30 pixels and less than 100 pixels (objects existing on scales 1, 2, and 3) with a retention rate of 74% and for cloud objects of 100+ pixels exhibiting a retention rate of 81%.

In summary, as the temporal resolution of the geostationary imager increases, the object tracking system performance improves. Twenty minute and larger scan gaps with GOES data can significantly decrease system performance. In addition, object tracking performance increases as object size increases and object tracking lifetime increases as cloud-objects reach higher into the troposphere. These two points give confidence that the objects of greatest interest (i.e., those that begin to develop into and have developed into thunderstorms) have the highest likelihood of successful tracking.

4. Application of convective cloud object tracking methodology

a. Example of fusing convective cloud object tracking output and meteorological fields

After the cloud object postprocessing routine is complete, the final merged cloud objects can be used as a vehicle to fuse any meteorological datasets for a wide array of potential utilities, especially for monitoring temporal trends of cloud object and meteorological properties. UW-CIMSS has developed an additional statistical postprocessing system that uses convective cloud objects to fuse raw satellite observations, satellite algorithm output [e.g., UWCI-CTC rate (Sieglaff et al. 2011), GOES cloud phase (Pavolonis and Heidinger 2004; Pavolonis et al. 2005; Pavolonis 2010a), GOES cloud height (Heidinger 2011), GOES visible optical depth and effective radius (Walther and Heidinger 2012)], NEXRAD observations and derived output (Lakshmanan et al. 2006) [e.g., base reflectivity, composite reflectivity, vertically integrated liquid (VIL), maximum expected size of hail (MESH)], NWP model fields and derived parameters, National Lightning Detection Network (NLDN) data (Cummings et al. 1998), and Storm Prediction Center (SPC) storm reports. The focus of this paper is not to provide technical details on the statistical postprocessing system, but rather to demonstrate the utility and ease of fusing meteorological data using the convective cloud object tracking system output.

On a high level, the statistical postprocessing system is simply a data structure with a unique entry for each cloud object ID number. For each cloud object (data structure entry), any number of statistics for any number of meteorological (or nonmeteorological) data fields and object-related metadata can be stored. For example, each data structure entry might include the first time and last time that an object exists, as well as histograms of different satellite, radar, and NWP fields for each time the object was present or at the temporal resolution of the respective meteorological field. From these histograms it is possible to compute and extract information such as the first time that specific radar thresholds are attained for a given cloud object, the time rate of change of different satellite observations and derived products, and when the first NLDN strike was detected within a cloud object.

Figure 6a shows the final merged cloud object output from the convective cloud object tracking system for

---

[4] Cloud objects will always drop out from one GOES scan to the next because of cloud dissipation and cloud merging. Unless the retention rate is manually quantified, the absolute values of the retention rates are difficult to interpret.
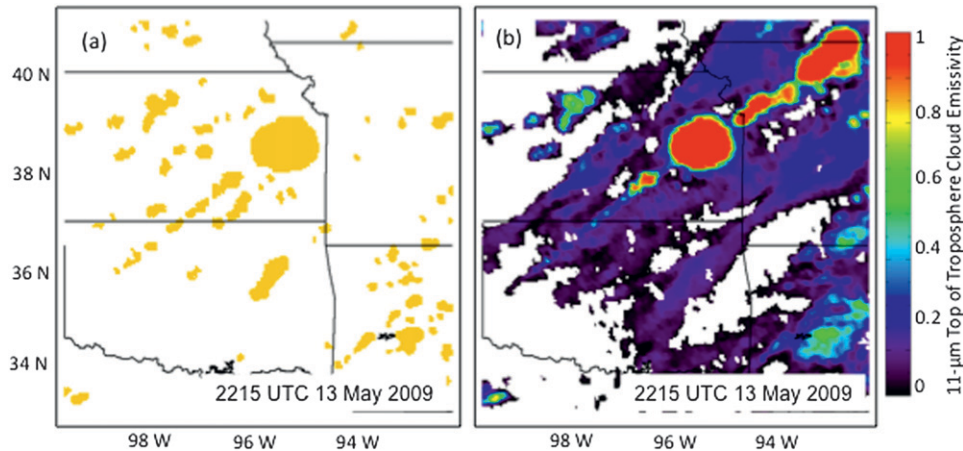
FIG. 6. (a) Final merged cloud objects and (b) 11-μm top-of-troposphere cloud emissivity field valid at 2215 UTC 13 May 2009 used as input into the convective cloud object tracking system. Final cloud objects are also used in Figs. 7–9.

2215 UTC 13 May 2009 over the central plains of the United States. The large object over eastern Kansas is a maturing supercell thunderstorm with a line of developing convective clouds extending to the southwest into south-central Kansas and northwestern Oklahoma. Northeast of the cell, over northwestern Missouri, the cloud objects have been purged because they have grown in excess of the user-defined 1000-pixel maximum size threshold described in section 3b(1) (recall the goal of monitoring growth of convective clouds, while important, this system is not designed to monitor a convective system through its entire life cycle). The ε_{tot} panel in Fig. 6b is shown as a reference from which the cloud objects were built.

Figure 7 illustrates how NEXRAD fields are fused into the cloud objects by the statistical postprocessing system. Quality-controlled NEXRAD data from the National Severe Storms Laboratory (NSSL; Lakshmanan et al. 2007a) is remapped from its native 0.01° horizontal resolution to a 0.04° latitude/longitude grid to match the satellite grid while retaining the 9 × 9 neighborhood maximum of the original data at each coarsened point. Figures 7a,c show cloud objects from Fig. 6a outlined in gray with composite radar reflectivity and VIL valid at 2216 UTC 13 May 2009 shaded, respectively. Figures 7b,d demonstrate data fusion of cloud objects filled by the maximum of the composite reflectivity and VIL fields, respectively. The supercell thunderstorm over eastern Kansas has a maximum composite reflectivity in excess of 70 dBZ (maximum VIL in excess of 70 kg m^{-2}), while the developing convective clouds to the southwest have a maximum composite reflectivity values ranging from 20 to 55 dBZ (maximum VIL ranges from 0 to 15 kg m^{-2}). The intense composite reflectivity to the northeast of the

supercell thunderstorm in eastern Kansas is not shaded on the cloud object plots because those objects exceeded the maximum size threshold and were pruned. These radar fields are presented purely as examples; any meteorological data field or, more generically, any georeferenced data field can be included and tracked within these cloud objects.

Figure 8 demonstrates how additional meteorological data are fused into the cloud object output. Figures 8a,c have cloud objects from Fig. 6a outlined in gray with NLDN lightning strikes colored by age prior to 2215 UTC 13 May 2009 and the Rapid Update Cycle (RUC; Benjamin et al. 1994) most unstable CAPE (MUCAPE) shaded and valid at 2200 UTC 13 May 2009, respectively. Figures 8b,d demonstrate data fusion of cloud objects filled by the elapsed time since the first NLDN strike and by maximum RUC MUCAPE, respectively. The supercell thunderstorm over eastern Kansas is shown to have the first NLDN strike 45 min prior to 2215 UTC (it may be useful to compare the first lightning strike time to time trends of satellite and radar observations), while the developing convection to the southwest has yet to produce an NLDN-detected lightning strike. The supercell thunderstorm over eastern Kansas and developing line to the southwest exist in a ribbon of locally high RUC MUCAPE (generally 3500+ J kg^{-1}), while cloud objects to the north and west behind the surface cold front (not shown) over central and northern Kansas have much smaller values of MUCAPE.

Figure 9 demonstrates how combining the 2D object tracking can be used to monitor temporal trends of any meteorological field of interest. Figure 9 shows the temporal trends of quantities related to deep convection
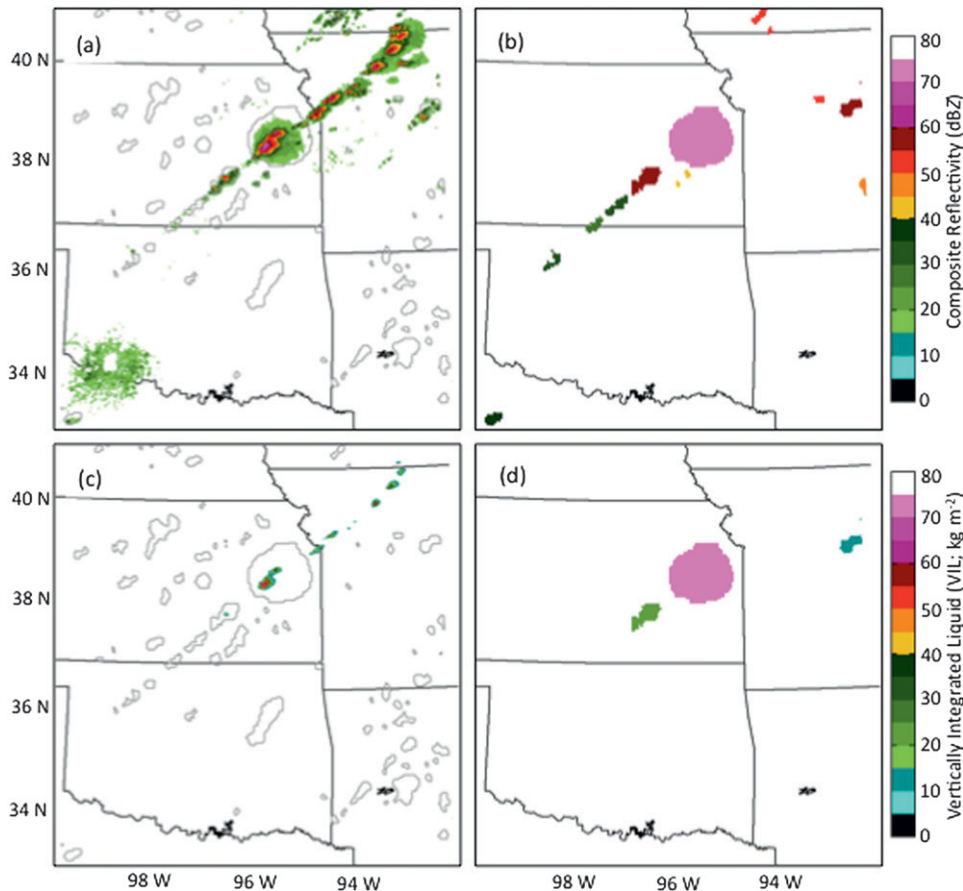
FIG. 7. (a) Final merged cloud objects from Fig. 6 (gray contours) valid at 2215 UTC 13 May 2009 are displayed with NEXRAD composite reflectivity (dBZ) and (c) NEXRAD VIL (kg m^{-2}) valid at 2216 UTC 13 May 2009. (b),(d) Cloud objects fused with NEXRAD composite reflectivity and VIL from (a),(c), respectively. Maximum composite reflectivity is shaded in (b) for objects that have a valid composite reflectivity, while cloud objects that have a valid VIL value are shaded according to their maximum in (d).

for three convective clouds from Figs. 6–8. Each colored line in Fig. 9 represents data for a specific cloud object identified in Fig. 8. All three storms exhibit rapidly cooling minimum *GOES-12* IR BTs at some point during their growth stage, followed by subsequent intensification of precipitation as characterized by the increased composite reflectivity. All three storms exhibited a first NLDN-detected lightning strike when *GOES-12* IR BTs reached the lower 220-K range (not implying this is always the case), but each storm had significantly different composite reflectivity at those first NLDN strike times. Note cloud object ID number 1 (Figs. 8, 9) was not detected until fairly cold GOES IR BTs were observed (~245 K); this is because the GOES satellite was operating in "full disk" mode between 2045 and 2115 UTC and most of the early development of this cloud occurred during the 30-min scan gap. Figure 9b highlights the maximum radar-estimated MESH (solid

lines) and median RUC MUCAPE (dashed lines) for the same set of storms in Fig. 9a. These three storms all produced radar-estimated severe hail (the east-central Kansas storm peaked at a MESH of 3.0+ in.). The two northern storms over Kansas exhibited median RUC MUCAPE between 3500 and 4000 J kg^{-1} (cloud object ID numbers 1 and 2; Figs. 8, 9), while the southern storm (cloud object ID number 3; Figs. 8, 9) exhibited values over 5000 J kg^{-1} with no appreciable temporal trends in the amount of instability. Thus, Fig. 9 motivates one potential utility of the system in which temporal relationships between many different meteorological fields can be investigated. For example, one could use the system to analyze the magnitude of *GOES-12* IR BT cooling rates versus the subsequent development of NEXRAD and/or NLDN observations constrained by various thresholds of environmental variables, such as NWP data and rawinsonde-derived fields.
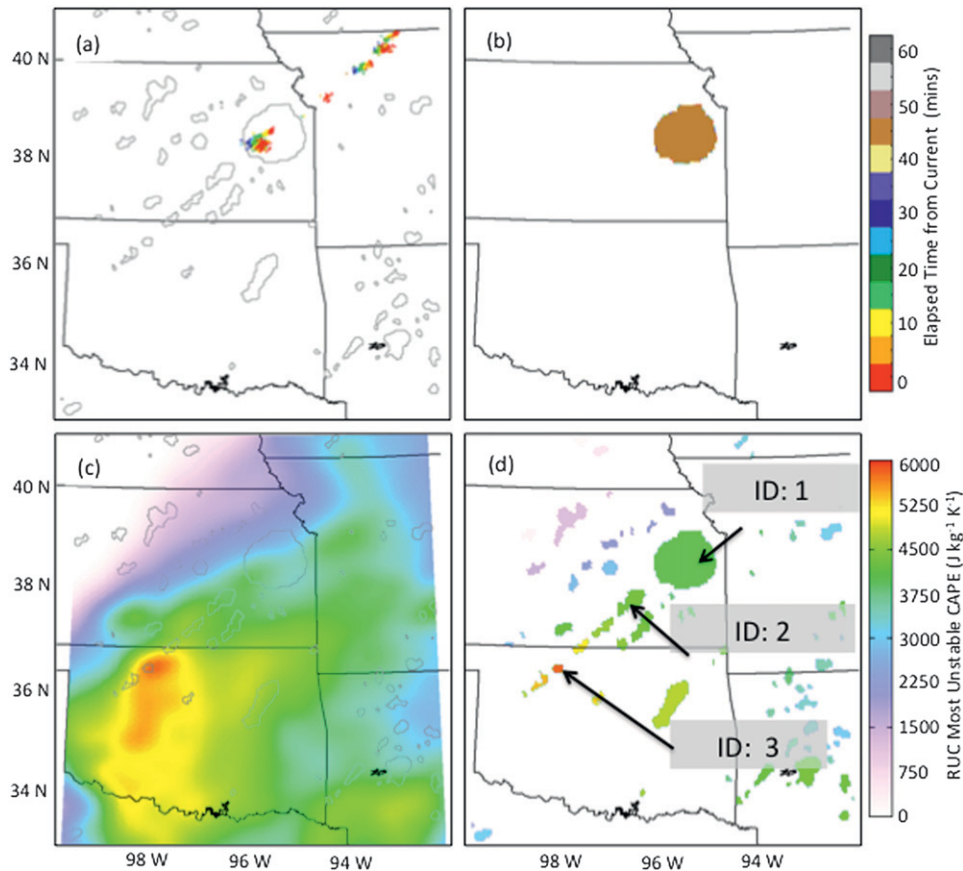
FIG. 8. (a) Final merged cloud objects from Fig. 6 (gray contours) valid at 2215 UTC 13 May 2009 are displayed with NLDN lightning strikes valid from 2115–2215 UTC 13 May 2009 and (c) MUCAPE (J kg^{-1}) valid at 2200 UTC 13 May 2009. (b),(d) Cloud objects fused with NLDN lightning strike data and RUC MUCAPE from (a),(c), respectively. The elapsed time (min) from 2215 UTC since an object's first detected lightning strike is shaded in (b), while cloud objects that have a valid RUC MUCAPE value are shaded according to their maximum in (d), which also includes cloud object ID tags for use with Fig. 9.

b. Application of cloud object tracking system at UW-CIMSS

Two research projects at UW-CIMSS currently utilize the convective cloud object tracking and statistical postprocessing systems. The first, described briefly in section 3b(2), uses the cloud object tracking system to determine the relationships between UWCI-CTC rates and a variety of NEXRAD fields and first NLDN strikes. The cloud object tracking system was used to determine the performance of the UWCI-CTC rates as a function of different NEXRAD fields. One key finding was that more intense UWCI-CTC rates were positively correlated with more intense precipitation cores in the future. In addition, a lead-time analysis of cloud-top cooling rates as a function of the same NEXRAD fields was generated to highlight the prognostic value of satellite-based cooling rates in operational forecasting. Such an in-depth analysis is not presented in this text, but the reader is referred to Hartung et al. (2013) for complete details. A second research project leverages the two systems to compute the time rate of change of an array of satellite cloud-retrieved fields (e.g., ε_{tot}, cloud phase, visible optical depth), combined with NWP data and NEXRAD data to probabilistically nowcast the likelihood that a developing convective cloud will produce surface severe weather reports in the subsequent 0–2-h time frame. The lead time of such probabilistic nowcasts ahead of severe weather warnings and radar indicated severe signatures are also being computed.

5. Conclusions

Deep convective clouds develop on small spatial and temporal scales (minutes to hours). To monitor the growth of convective clouds from infancy into the mature phase, it is necessary to observe these clouds with sufficiently
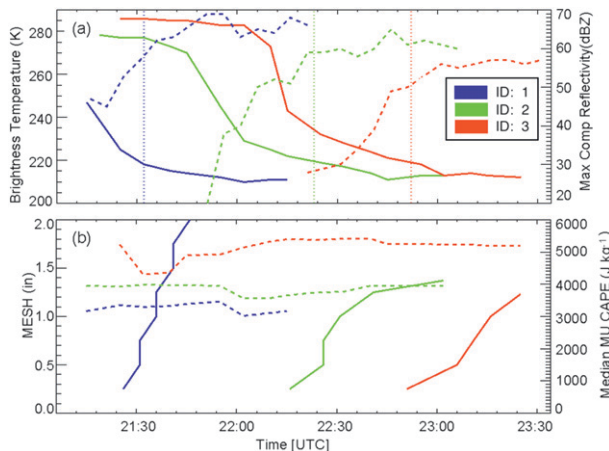
FIG. 9. Time series of various meteorological properties for three cloud objects from 13 May 2009 (Figs. 6–8). Blue lines are for cloud object ID number 1 in east-central Kansas (see Fig. 8 for cloud object ID labels), green lines are for cloud object ID number 2 to the southwest of the blue storm, and red lines are for cloud object ID number 3 near the Kansas–Oklahoma border. (a) Time series of minimum *GOES-12* IR window BTs (solid lines), maximum NEXRAD composite reflectivity (dashed lines), and first NLDN-detected lightning strike (vertical dotted lines). (b) Time series of maximum radar-based MESH (solid lines) and median object RUC MUCAPE (dashed lines).

high spatial and temporal resolution. Geostationary imagers and NEXRAD are two such remote sensing platforms that yield this type of high-quality data. When using these observational datasets, human analysts do not view individual pixels, but rather individual convective towers or storms (groups of pixels). With the goal of mimicking a human's subjective interpretation of cloud objects in an objective automated manner, UW-CIMSS has developed a convective cloud object tracking system that utilizes the WDSS-II framework developed at the University of Oklahoma to group adjacent cloudy satellite pixels into cloud objects, similar to how a human would analyze satellite or radar data and track these cloud objects through space and time. A UW-CIMSS postprocessing utility then merges the WDSS-II output and performs steps to minimize the broken tracks of convective cloud objects. The convective cloud object tracking system presented herein is designed to track convective clouds from infancy into the mature phase and provide a means to generate statistics of any number of meteorological fields, as well as temporal trends of such fields for each cloud object within a time period of interest.

The convective cloud object tracking system uses the 11-μm top-of-troposphere cloud emissivity (ε_{tot}) as input into WDSS-II for cloud object identification and tracking. The input ε_{tot} field is derived using only 11-μm IR radiances (or equivalent), and thus the system is

capable of operating both day and night for any geostationary imager with sufficient temporal resolution. The UW-CIMSS-developed postprocessing system combines three different size scale outputs from WDSS-II into a final set of cloud objects, minimizing broken cloud tracks in the process.

The analysis of the convective cloud object tracking system performance revealed that 1) the cloud object tracking performance increases with improved imager temporal resolution; 2) the larger an object grows, the better the cloud object tracking system performs (key for tracking cumulus with vertical growth and newly developed cumulonimbus); and 3) cloud objects that grow higher in the troposphere (i.e., thunderstorms) are tracked longer than cloud objects that remain in the lower troposphere (i.e., shallow cumulus). While not discussed within the text, it should be noted that the typical Linux research system run time on a domain covering the central and eastern CONUS and adjacent oceanic regions is approximately 6 min per satellite scan, which suggests that this system has the potential to be used in real-time applications.

Since cloud objects are output on a 0.04° grid, it is straightforward to fuse a variety of meteorological data fields into one framework by projecting the data onto the same grid. With the use of a statistical postprocessing system, the cloud object output can be used to fuse raw satellite observations, satellite derived/retrieved fields, NEXRAD observations and algorithm output, NWP fields, NLDN data, and SPC storm reports. In fact, any georeferenced dataset, including nonmeteorological data, can be fused with the cloud objects through the statistical postprocessing system with the ability to monitor temporal trends in all data fields. Two research projects at UW-CIMSS are utilizing the convective cloud object tracking system and publications from those projects will further demonstrate the utility of the system (e.g., Hartung et al. 2013).

REFERENCES

Aminou, D. M. A., 2002: MSG's SEVIRI instrument. *ESA Bull.,* **111,** 15–17.
Benjamin, S. G., K. A. Brewster, R. L. Brummer, B. F. Jewett, T. W. Schlatter, T. L. Smith, and P. A. Stamus, 1991: An isentropic three-hourly data assimilation system using ACARS aircraft observations. *Mon. Wea. Rev.,* **119,** 888–906.

——, K. J. Brundage, and L. L. Morone, 1994: The Rapid Update Cycle. Part I: Analysis/model description, NOAA/NWS Tech. Procedures Bull. 416, 16 pp.

Carvalho, L. M. V., and C. Jones, 2001: A satellite method to identify structural properties of mesoscale convective systems based on the Maximum Spatial Correlation Tracking Technique (MASCOTTE). *J. Appl. Meteor.,* **40,** 1683–1701.

Cummings, K. L., M. J. Murphy, E. A. Bardo, W. L. Hiscox, R. B. Pyle, and A. E. Pifer, 1998: A combined TOA/MDF technology upgrade of the U.S. National Lightning Detection Network. *J. Geophys. Res.,* **103** (D8), 9035–9044.

Dixon, M., and G. Wiener, 1993: TITAN: Thunderstorm Identification, Tracking, Analysis and Nowcasting—A radar-based methodology. *J. Atmos. Oceanic Technol.,* **10,** 785–797.

Hartung, D., J. Sieglaff, L. Cronce, and W. Feltz, 2013: An intercomparison of UW cloud-top cooling rates with WSR-88D radar data. *Wea. Forecasting,* in press.

Heidinger, A. K., 2010: ABI cloud mask algorithm theoretical basis document. NOAA/NESDIS/Center for Satellite Applications and Research (STAR), 67 pp.

——, 2011: ABI cloud height algorithm theoretical basis document. NOAA/NESDIS/Center for Satellite Applications and Research (STAR), 77 pp.

Hillger, D. W., and T. J. Schmit, 2007: The GOES-13 science test: Imager and sounder radiance and product validations. NOAA Tech. Rep. NESDIS 125, 88 pp.

Johns, R. H., and C. A. Doswell III, 1992: Severe local storms forecasting. *Wea. Forecasting,* **7,** 588–612.

Kanamitsu, M., 1989: Description of the NMC Global Data Assimilation and Forecast System. *Wea. Forecasting,* **4,** 335–342.

Lakshmanan, V., and T. Smith, 2010: An objective method of evaluating and devising storm-tracking algorithms. *Wea. Forecasting,* **25,** 701–709.

——, R. Rabin, and V. DeBrunner, 2003: Multiscale storm identification and forecast. *J. Atmos. Res.,* **67–68,** 367–380.

——, T. Smith, K. Hondl, G. J. Stumpf, and A. Witt, 2006: A real-time, three-dimensional, rapidly updating, heterogeneous radar merger technique for reflectivity, velocity, and derived products. *Wea. Forecasting,* **21,** 802–823.

——, A. Fritz, T. Smith, K. Hondl, and G. J. Stumpf, 2007a: An automated technique to quality control radar reflectivity data. *J. Appl. Meteor. Climatol.,* **46,** 288–305.

——, T. Smith, G. J. Stumpf, and K. Hondl, 2007b: The Warning Decision Support System–Integrated Information. *Wea. Forecasting,* **22,** 596–612.

——, K. Hondl, and R. Rabin, 2009: An efficient general-purpose technique for identifying storm cells in geospatial images. *J. Atmos. Oceanic Technol.,* **26,** 523–537.

Leone, D. A., R. M. Endlich, J. Petriceks, R. T. H. Collins, and J. R. Porter, 1989: Meteorological considerations used in planning the NEXRAD network. *Bull. Amer. Meteor. Soc.,* **70,** 4–13.

Menzel, P., and J. Purdom, 1994: The first of a new generation of geostationary operational environmental satellites. *Bull. Amer. Meteor. Soc.,* **75,** 757–782.

Moller, A. R., 2001: Severe local storms forecasting. *Severe Convective Storms, Meteor. Monogr.,* No. 50, Amer. Meteor. Soc., 433–480.

Morel, C., F. Orain, and S. Senesi, 1997: Automated detection and characterization of MCS using the Meteosat infrared channel. *Proc. Meteorological Satellite Data User's Conf.,* Brussels, Belgium, EUMETSAT, 213–220.

——, S. Sénési, and F. Autones, 2002: Building upon SAF-NWC products: Use of the rapid developing thunderstorms (RDT) product in Météo-France nowcasting tools. *Proc. Meteorological Satellite Data Users' Conf.,* Dublin, Ireland, EUMETSAT and Met Eirean, 248–255.

NEXRAD, 1985: Next Generation Weather Radar (NEXRAD) algorithm report. NEXRAD Joint System Program Office Rep. R400-AR301, 926 pp.

Pavolonis, M. J., 2010a: ABI cloud type/phase algorithm theoretical basis document. NOAA/NESDIS/Center for Satellite Applications and Research (STAR), 60 pp.

——, 2010b: Advances in extracting cloud composition from spaceborne radiances: A robust alternative to brightness temperatures. Part I: Theory. *J. Appl. Meteor. Climatol.,* **49,** 1992–2012.

——, and A. K. Heidinger, 2004: Daytime cloud overlap detection from AVHRR and VIIRS. *J. Appl. Meteor.,* **43,** 762–778.

——, ——, and T. Uttal, 2005: Daytime global cloud typing from AVHRR and VIIRS: Algorithm description, validation, and comparisons. *J. Appl. Meteor.,* **44,** 804–826.

Puschell, J. J., and Coauthors, 2002: Japanese Advanced Meteorological Imager: A next generation GEO imager for MTSAT-1R. *Earth Observing Systems VII,* W. L. Barnes, Ed., International Society for Optical Engineering (SPIE Proceedings, Vol. 4814), doi:10.1117/12.453755.

Roberts, R. D., and S. Rutledge, 2003: Nowcasting storm initiation and growth using *GOES-8* and WSR-88D data. *Wea. Forecasting,* **18,** 562–584.

Root, B., M. Yeary, and T.-Y. Yu, 2011: Novel storm cell tracking with multiple hypothesis tracking, Preprints, *27th Conf. on Interactive Information Processing Systems (IIPS),* Seattle, WA, Amer. Meteor. Soc., 8B.3. [Available online at http://ams.confex.com/ams/91Annual/webprogram/Manuscript/Paper184250/AMSAnnual2011_MHTAbstract.pdf.]

Schmit, T. J., M. M. Gunshor, W. P. Menzel, J. J. Gurka, J. Li, and A. S. Bachmeier, 2005: Introducing the next-generation Advanced Baseline Imager (ABI) on GOES-R. *Bull. Amer. Meteor. Soc.,* **86,** 1079–1096.

Sieglaff, J. M., L. M. Cronce, W. F. Feltz, K. M. Bedka, M. J. Pavolonis, and A. K. Heidinger, 2011: Nowcasting convective storm initiation using satellite-based box-averaged cloud-top cooling and cloud-type trends. *J. Appl. Meteor. Climatol.,* **50,** 110–126.

Vila, D. A., L. A. T. Machado, H. Laurent, and I. Velasco, 2008: Forecast and Tracking the Evolution of Cloud Clusters (ForTraCC) using satellite infrared imagery: Methodology and validation. *Wea. Forecasting,* **23,** 233–245.

Wallace, J., and P. Hobbs, 1977: *Atmospheric Science: An Introductory Survey.* Academic Press, 467 pp.

Walther, A., and A. Heidinger, 2012: Implementation of the Daytime Cloud Optical and Microphysical Properties Algorithm (DCOMP) in PATMOS-x. *J. Appl. Meteor. Climatol.,* **51,** 1371–1390.

Zinner, T., H. Hammstein, and A. Tafferner, 2008: Cb-TRAM: Tracking and monitoring severe convection from onset over rapid development to mature phase using multi-channel Meteosat-8 SEVIRI data. *Meteor. Atmos. Phys.,* **101,** 191–210.